Scale-model Scattering Experiments using 3D Printed Representations of Ocean Bottom Features

David C. Calvo, Michael Nicholas,
Joseph M. Fialkowski, Roger C. Gauss
Acoustics Division, Code 7160
Naval Research Laboratory
Washington, DC 20375, USA

Derek R. Olson
Applied Research Laboratory
The Pennsylvania State University
State College, PA 16804, USA

Anthony P. Lyons
Center for Coastal and Ocean Mapping
The University of New Hampshire
Durham, NH 03824, USA

***Abstract*—This study examines tank measurements of acoustic backscatter from different scale-model representations of ocean bottom features. The emphasis is on comparing backscatter from a periodic, rippled surface made from machinable blue wax vs. identical surface geometries made using a 3D printer. The dominant features of the echoes obtained over 85 deg of monostatic angles are found to be similar for sufficiently thick prints beyond approximately 25 deg incidence angles. Acoustic backscatter is also presented for a 3D printed representation of an underwater rock outcrop surveyed in Larvik, Norway using an interferometric SAS system.**

I. Introduction

Ultrasonic tank experiments using scale models have been used in the past to validate underwater acoustic computational propagation models for sloping geometries (e.g., [1]–[6]). Most studies have used calibrated sand or in some cases epoxy to mimic an ocean sediment layer. Recent efforts have considered three-dimensional propagation effects by milling polyurethane foam into scale models of actual ocean bathymetry such as canyons [7], [8]. The foam truncates the ocean bottom by treating it as a pressure release boundary. In terms of penetrable elastic ocean bottoms, scale models for propagation in sloping environments have been achieved by angling polyvinyl chloride (PVC) slabs underwater [9]. Transmission loss measured for these penetrable slab experiments have been useful for validating elastic parabolic equation methods. In all these cases, precisely controlled experiments serve as a useful alternative, and also a complement, to full-wave numerical simulations that often require high-performance computing resources particularly for three-dimensional environments.

Tank experiments have also been used to examine acoustic backscatter from rough surfaces (e.g., [10]–[12]). In the latter case of work done at the Naval Research Laboratory (NRL), statistically rough surfaces were milled from PVC using a process described in [13]. As part of the same effort, rippled scale models that mimicked periodic sandbars were also made using soft machinable blue wax [14], [15]. The milling approaches mentioned are examples of subtractive manufacturing processes in which material is removed. The present study considers ocean bottom representations made using the additive manufacturing process commonly known as 3D printing. This process allows for rapid prototyping of scale models. Two sample geometries are shown in Fig. 1.

The objectives of the present work are to identify differences in backscatter features between blue wax and 3D printed surface geometries, and to examine what printed thicknesses are sufficient to approximate a half-space. The study is organized as follows. The rippled reference profile, experimental setup, and material properties are first summarized. Backscatter time series are then compared for blue wax vs. the thicker of two printed samples for the rippled geometry. Time series from the two printed samples are then

Fig. 1. Examples of 3D printed geometries. A 1/67 scale representation of a 15 m long rock outcrop from Larvik, Norway is in the foreground, and a rippled surface of 304 mm side length is in the background.

Work sponsored by the Office of Naval Research.

compared. This information is useful to determine the extent that results for 3D printed plastic can be extrapolated to other materials such as the softer blue wax or, on the other extreme, hard materials such as rock. In cases where scaling is poor, 3D printing can be used as a stage in a molding process for materials such as concrete or wax [16], [17]. Finally, as an example of a more complex ocean boundary, backscatter measurements are presented for a 3D printed representation of an undersea rock outcrop surveyed in Larvik, Norway using an interferometric synthetic aperture sonar system [18]–[21]. The 1/67 scale model is shown in Fig. 1.

II. Rippled Surfaces

A. Surface Profile

The periodic rippled surface profile used was inspired by sandbar geometries that form naturally in shallow water due to water wave action [22]. The surface height $z=f(x)$ used in this study is

$$z = hu^p, \tag{1}$$

where

$$u = \frac{1}{2} + \frac{1}{2}\cos\left(2\pi(x - L_0)/L\right), \tag{2}$$

and

$$p = \frac{1}{1 - \log_2\left(\cos(2\pi w/L) + 1\right)}. \tag{3}$$

The surface height is given by h = 10 mm, ripple separation L=50 mm, width parameter w = 6.75 mm, and shift parameter L_0=17 mm. The width parameter w is the half-width of a ripple at half-amplitude. The model geometry extends over the interval [0, 304 mm]. A plot is shown in Fig. 2. The surface profile has a peak surface slope of 47.2°. The phase shift parameter was chosen arbitrarily and simply corresponds to a sample that was available from a previous NRL effort.

The original blue wax sample considered in [14] had a ripple height of one wavelength at 500 kHz. That relatively short-ripple sample appears similar to that shown in Fig. 2(b) of [15]. The blue wax sample used in the present study has a ripple height of 7 wavelengths at 1 MHz to provide a relatively larger geometry than before that is more comparable to a rock outcrop.

B. Fabricated Samples

The fabricated samples are shown in Fig. 3. The light blue samples were printed with a photopolymer called VeroBlue. The samples are square when seen from above with side length 304 mm (approximately 1 ft). In terms of adding the height profile in Fig. 2 to a constant base slab thickness, the base slabs are 39.5 mm thick for the blue wax sample, 20 mm thick for the first VeroBlue sample, and 10 mm for the thin VeroBlue sample. The two VeroBlue samples were created to assess the required thickness to approximate an elastic half-space. The machinable blue wax (Freeman Manufacturing & Supply Company, Ohio) was milled using a reduced dimension version of the process described in [13].

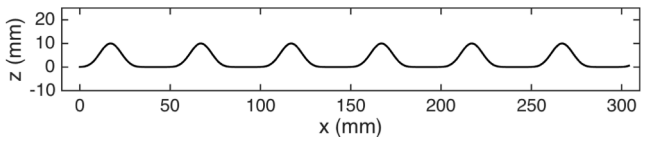

Fig. 2. The rippled surface profile used in this study.

Fig. 3. Fabricated rippled samples used in this study. Machinable blue wax (left) shown with 3D printed (VeroBlue) samples with thick base (middle) and thin base (right). The length of the ruler in the foreground is 150 mm.

The printed samples were made using the Polyjet process of jetting and then UV-curing a liquid photopolymer for layer-by-layer fabrication [23]. VeroBlue RGD840 was selected as the material for use in an Objet500 Connex printer (Stratasys, Minnesota). The cured material resembles plastic and was printed in a high-quality (as opposed to fast) setting. When smaller test samples were intentionally fractured, no directional or nonuniform microstructure was visible to the unaided eye on the newly exposed areas. Although the VeroBlue material data sheet indicates that it can absorb water, no observable changes in backscatter were noticed after 3 days of continuous immersion or over 2 months of periodic immersions and acoustic tests. This is likely due to the monolithic and bulk geometry of the sample that did not include elaborate or thin structures.

Print files in the STL format were generated starting first with a Cartesian surface height grid. The points were then read into a commercial software package (COMSOL Multiphysics) and an interpolation surface was defined. The surface was then used to divide a rectangular block used as a base. The top surface of the resulting sample volume was meshed with fine triangular elements, and the volume was meshed with tetrahedral elements of increasing size further away from the top surface. The rippled surface had a maximum triangular element size of 1.5 mm that produced approximately 120,000 triangular surface elements. The printed surface was smooth to touch with no evidence of triangular facets. The thick and thin VeroBlue samples took approximately 13 and 9 hours to print, respectively. The outcrop contained 150,000 triangular elements on its rough surface and took approximately 11 hours to print.

C. Material Properties

Measurements of most of the material properties of the

TABLE I. MATERIAL PROPERTIES

Material	Machinable Blue Wax (0.5 – 1.5 MHz)	VeroBlue RGD 840 (300 – 500 kHz)
Density	930 kg/m^3	1185 kg/m^3
Compression wave speed	1973 m/s	2250 m/s
Shear wave speed	772 m/s [a]	1140 m/s
Compression wave attenuation	5.75 dB/(cm MHz) (~ 1.1 dB//λ_p)	4.55 dB/(cm MHz) (~1.0 dB/λ_p)
Shear wave attenuation	n/a	22.5 dB/(cm MHz) (~2.6 dB/λ_s)

[a] Reference [17]

blue wax and VeroBlue are listed in Table 1. Both compression (p) and shear (s) wave speeds and attenuations were measured by underwater transmission measurements as described in [24], [25]. Over wide frequency ranges, elastic wave properties can commonly vary as a power law. The properties reported were measured over the restricted ranges indicated where attenuation scales linearly with frequency and phase speed dispersion is weak. In terms of a penetrable water-solid planar interface, both materials are soft in comparison with hard rock (e.g. basalt) since the shear wave speeds are significantly less than water which affects mode conversion [25].

III. EXPERIMENTAL SETUP

A. Geometry & Hardware

Tests were performed in a 4x4x4 ft^3 water tank at the Naval Research Laboratory. The geometry is depicted in Fig. 4 and an image is provided in Fig. 5. A piston transducer (Model V303, Panametrics/Olympus, Massachusetts) with an active element diameter of 0.5 in and a center frequency of 1 MHz was used as both the source and receiver. The source has a full beamwidth of 6.9° between -6 dB points at 1 MHz, and was driven by a Panametrics/Olympus 5077PR pulser operating at 300 volts. The source was positioned 30 cm from the sample base plane defined by zero ripple amplitude as indicated in Fig. 4(b). The center of the sample and piston were both located 22 in below the water surface. The sample was held in place by fiberglass jaws as indicated in Fig. 4(c). The source/receiver was kept fixed and the sample was rotated from 0 to 85° in 1° increments about a point on the base plane as indicated. The jaw structure was arranged so that at grazing incidence the beam did not scatter from the posts. The experiment was controlled through LabView which averaged 100 pings per angular position. Before measurements were taken, a water jet was used on all submerged surfaces to remove any possible bubbles that may have been trapped during the submersion process.

B. Pulse Waveform

The source output waveform was measured by rotating the source so that it aimed vertically upward at the water-air interface. The separation was adjusted to 30 cm (same as the distance to sample plane). The R = -1 reflection coefficient from the water-air interface means the reflected pulse is barely distorted aside from a 180° phase reversal. A time series of the inverted reflection and its frequency spectrum are plotted in Fig. 6. All time series throughout this study are low-pass filtered below 2.5 MHz. The waveform has a bandwidth of 600 kHz between -6 dB spectral intensity points.

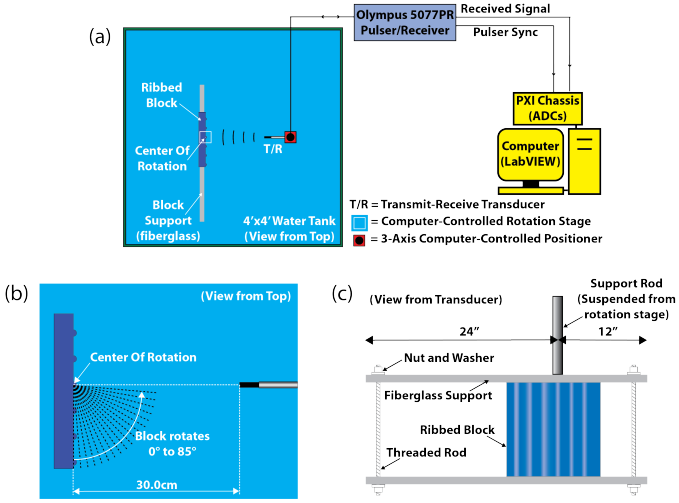

Fig. 4. Experimental setup driven by LabView. Piston is kept fixed, sample is rotated (a). Expanded view of sample with sense of rotation indicated (b). View of the sample and its holder frame as seen from the piston source (c).

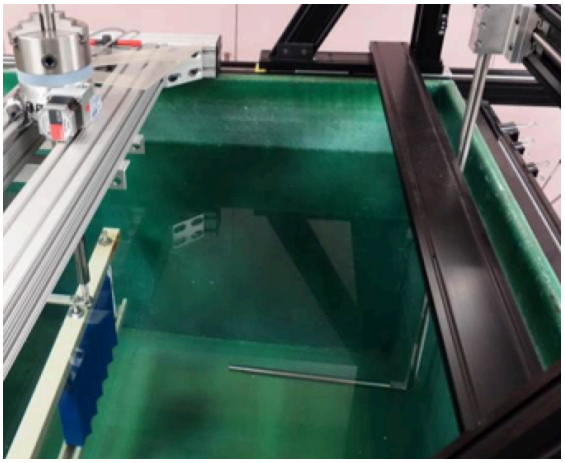

Fig. 5. Photograph of the experimental setup. The blue wax sample can be seen in the rotation stage.

IV. Backscatter Measurements

A. *Rippled Samples*

Fig. 7 compares backscatter time series for the three samples. While an elastic wave version of ray tracing through the sample and diffraction theory can be used to explain the features, in this paper only the major observable differences are reported to inform further developments of the methods. Most of the difference in structure occurs within 25° of normal incidence. Near 85° incidence (5° grazing), the echoes from the six ripples can be clearly identified at low levels with an extra echo from the front side of the slab arriving earliest. The final ripple echo in the blue wax case was too weak to be detected at the pulser voltage used. This is partly due to the compression wave impedance difference of the material (the wax is 0.69 the impedance of VeroBlue) and the fact that VeroBlue is more rigid than wax (has a much larger shear wave speed). In both VeroBlue cases, however, there is a significant difference in the final ripple echo at grazing incidence that suggests the thinner slab is too thin.

A zoomed view of the highest amplitude arrivals is shown in Fig. 8. All cases appear to show a thickness related feature that can be first seen near 0.545 ms and 10° in the blue wax case, but progressively shifts to earlier times in the VeroBlue cases, becoming strong at 0.515 ms in the thin case. In all cases, the strongest returns appear near 46° where the incident wave encounters a broad reflecting face near the change in ripple curvature.

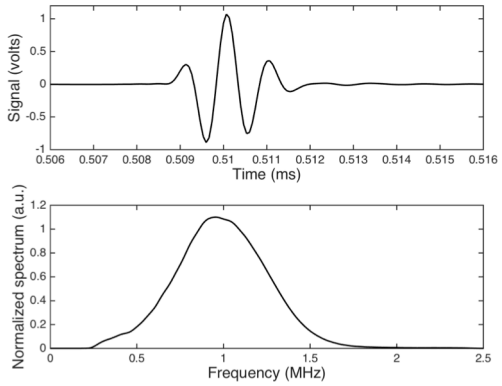

Fig. 6. Normal incidence reference pulse (measured voltage) reflected from the water-air interface at 30 cm distance (upper plot). Pulse has been low-pass filtered below 2.5 MHz. Normalized spectrum of pulse (lower plot).

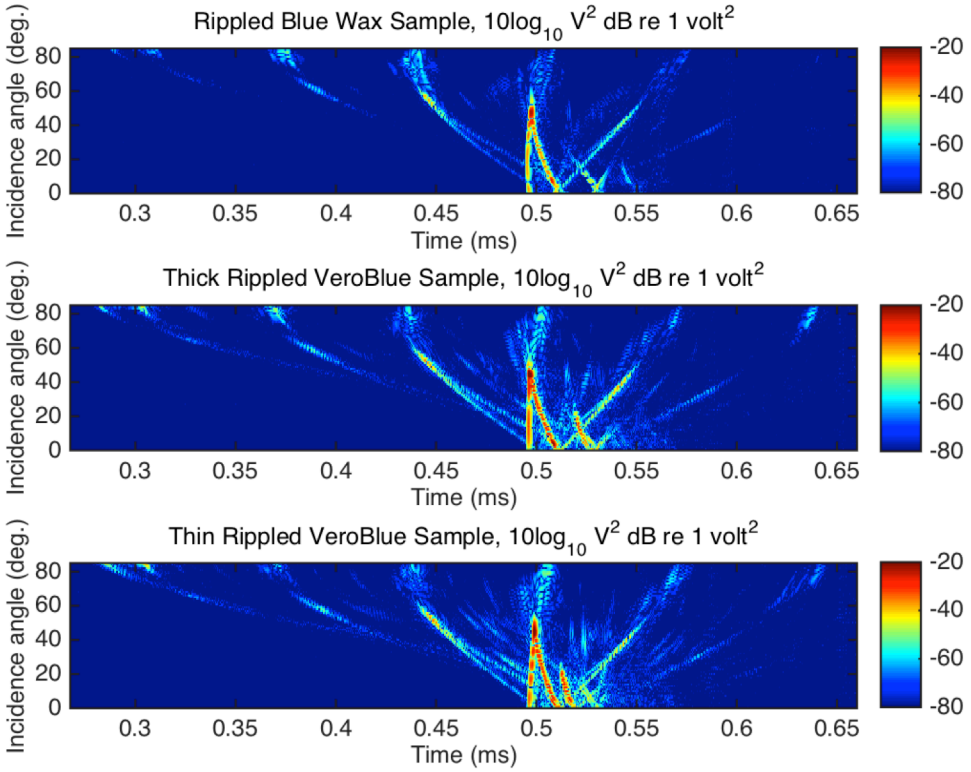

Fig. 7. Backscattered time series for the blue wax sample (top), thick VeroBlue sample (middle), and thin vero blue sample (bottom). All samples have identical surface shape.

A useful test is obtained by flipping a sample inside the test jaws. Boundary reverberation originating from within the sample that returns to the source is indicative of a sample thickness that may be too shallow for a particular range of incidence angles. This test is done using the thick rippled VeroBlue sample. An additional case considered is that of an unmilled blue wax block of 2 in thickness (parallel faces). Both cases are plotted in Fig. 9. In the latter case reverberation within the sample is expected to be very weak due to the flat faces. In the VeroBlue case, the normal incidence scattering appears relatively free from any diffuse component compared to its standard orientation in the lower panel of Fig. 8. The results in Fig. 9 indicate that beyond 20° incidence the back rippled structure is barely visible in the returns. In the ummilled blue wax case, reveberation is extremely weak off 0° incidence as expected.

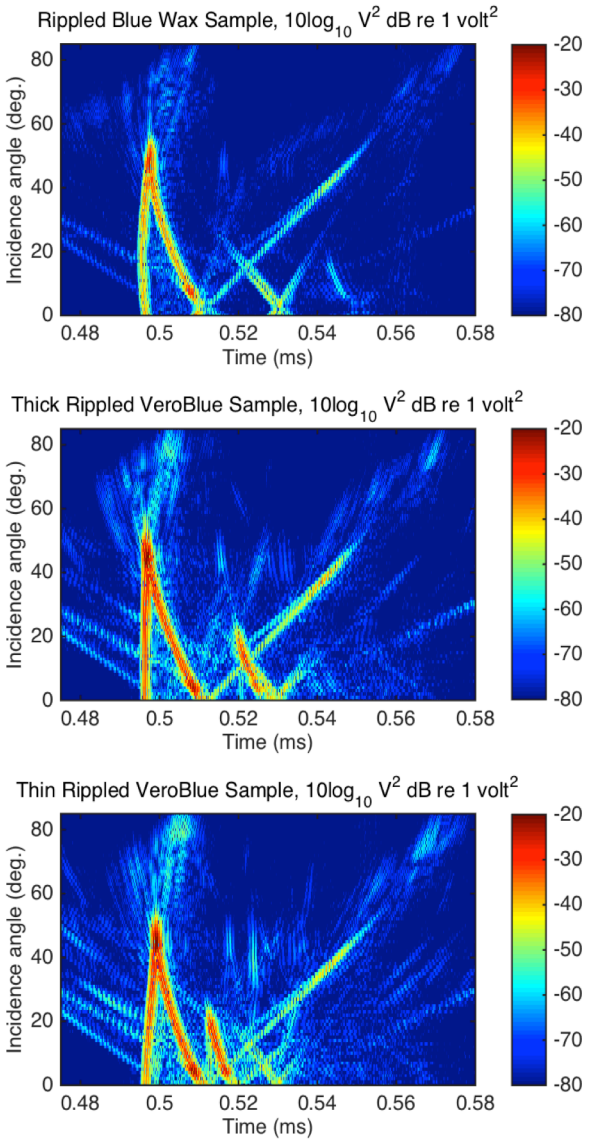

Fig. 8. Zoomed view of previous figure showing the scattering features. The main echo has a higher level in VeroBlue cases due to the higher impedance. A thickness related feature appears to migrate between 0.515 and 0.55 ms.

B. *VeroBlue Representation of the Rock Outcrop*

Although a complete examination of scattering from the rock outcrop shape is beyond the current study, examples of measurements and methods are provided. Fig. 10 shows the VeroBlue representation of the rock outcrop shape installed in a special holder. The geometry of the holder is designed so that the beam sweeps through 180° in the indicated plane as the rotation stage is actuated. The source/receiver is again stationary. It is noted that the shape is based on a limited coverage SAS dataset and so interpolation was necessary in some regions. This was easily handled by depopulating certain regions of the Cartesian point cloud read into the processing software which were then automatically interpolated when the surface representation was calculated. Fig. 11 shows the resulting backscatter time series over the angular space. The position of the sample in Fig. 10(a) corresponds to 0°. The strong echo at 180° in Fig. 11 is the broadside echo from the short side of the green frame. The gradual variation of features

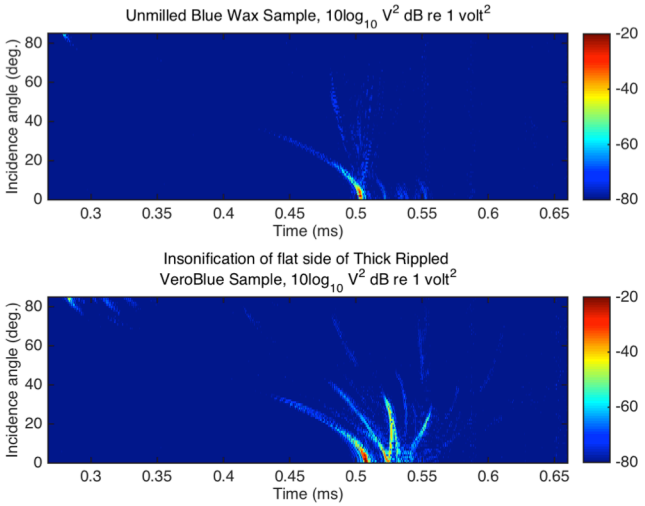

Fig. 9. (upper) Backscatter from an unmilled 2 in thick blue wax block (both of its faces are flat). (lower) Case of flipping the thick rippled VeroBlue sample so that the insonified face is flat and the back of the sample is rippled. Structures in the lower plot are echoes from back rippled face which is still effectively probed at the lower incidence angles.

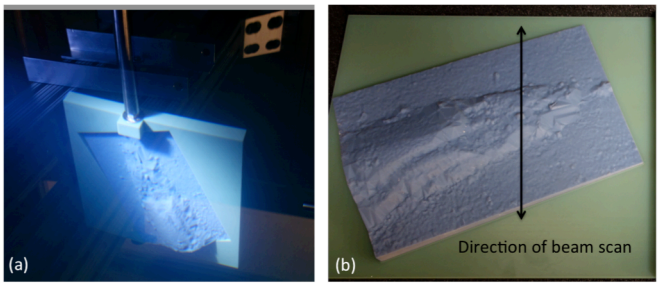

Fig. 10. (a) Photograph of the VeroBlue rock outcrop model positioned in the laboratory tank. The 0° position is shown with the piston just visible in the right part of photograph. Sample is inserted into a holder that is mounted to the rotation stage. (b) Acoustic beam is directed at an origin inside the sample and located in the transverse plane containing the black line. See Fig. 6 in [26] for origin and transect height profile at full scale.

suggests the importance of striations vs. a random background. Further study is being pursued in other NRL efforts [26].

V. Summary

This paper has presented a renewed effort on ultrasonic tank tests for boundary scatter studies being pursued at the Naval Research Laboratory. Starting with backscatter experiments using a milled blue wax sample from previous work, 3D printing was used to fabricate samples of identical surface shape but different thicknesses. The thickness required to approximate a half-space generally depends on the required dynamic range in dB which is related to other information such as the lateral extent of a surface. Measurements presented can be used as a reference point. For the particular VeroBlue rippled cases considered, for incidence angles larger than approximately 25°, difference were minor down to -60 dB level. Samples made using the Polyjet material/process appeared to be sufficiently uniform and free from processing artifacts. For the purposes and durations considered, water immersion of VeroBlue was not problematic. Although not covered in detail, backscatter measurements were observed to be repeatable to a high degree when tested over a multi-day period.

Acknowledgment

The rippled wax sample was created by Adith Ramamurti and Jason Summers at NRL in 2007 based on the surface profile provided by Robert Gragg. The measurements of elastic wave properties of VeroBlue were made by Christopher Layman at NRL. The authors would like to thank the Norwegian Defence Research Establishment (FFI), in conjunction with the Applied Research Laboratory, The Pennsylvania State University, for providing the bathymetric rock-outcrop data, and in particular Torstein O. Sæbø and Roy E. Hansen of FFI.

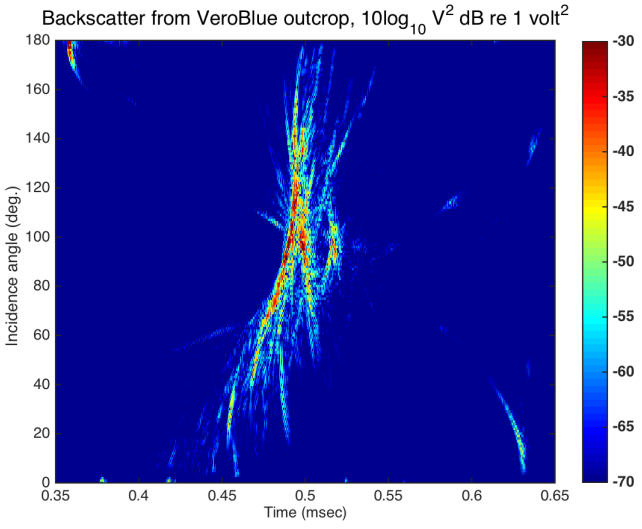

Fig. 11. Example measurements of backscatter from the rock outcrop surface representation for the aspect indicated in Fig. 10.

References

[1] J. R. Chamuel and G. H. Brooke, "Shallow water acoustic studies using an air-suspended water waveguide model," *J. Acoust. Soc. Am.,* vol. 84, no. 5, pp. 1777–1786, November 1988.

[2] S. A. L. Glegg, G. B. Deane, and I. G. House, "Comparison between theory and model scale measurements of three-dimensional sound propagation in a shear supporting penetrable wedge", *J. Acoust. Soc. Am.*, vol. 94, no. 4, pp. 2334–2342, October 1993.

[3] M. A. Ainslie, L. S. Wang, C. H. Harrison, and N. G. Pace, "Numerical and laboratory modeling of propagation over troughs and ridges", *J. Acoust. Soc. Am*., vol. 94 , no. 4, pp. 2287–2295, October 1993.

[4] J.-P. Sessarego, "Scaled models for underwater acoustics and geotechnics applications," in *Proceedings of the Sixth European Conference on Underwater Acoustics: ECUA 2002*, Gdansk, Poland, June 2002, pp. 209–216.

[5] A. Korakas, F. Sturm, J.-P. Sessarego, and D. Ferrand, "Scaled model experiment of long-range across-slope pulse propagation in a penetrable wedge," *J. Acoust. Soc. Am.*, vol. 126, no. 1, pp. EL22-EL27, July 2009.

[6] F. Sturm and A. Korakas, "Comparisons of laboratory scale measurements of three-dimensional acoustic propagation with solutions by a parabolic equation model," *J. Acoust. Soc. Am.*, vol. 133, no. 1, pp. 108–118, January 2013.

[7] J.D. Sagers, "Three-dimensional scale-model tank experiment of the Hudson Canyon Region," The University of Texas at Austin Applied Research Laboratory, Annual Report, September 2013.

[8] J.D. Sagers, "Results from a scale model acoustic propagation experiment over a translationally invariant wedge," *Proceed. of Meetings on Acoustics*, vol. 22, December 2014, p. 070001.

[9] J.M. Collis, W.L. Siegmann, M.D. Collins, H.J. Simpson, and R.J. Soukup, "Comparison of simulations and data from a seismo-acoustic tank experiment," *J. Acoust. Soc. Am.*, vol. 122, no. 4, pp. 1987–1993, October 2007.

[10] K.M. Becker, "Effect of various surface-height-distribution properties on acoustic backscattering statistics", *IEEE J. Ocean. Eng.*, vol. 29, no. 2, pp. 246–259, April 2004.

[11] J.-P. Sessarego, "Use of scaled models to study scattering by rough bottoms: Application to sea floor backscattering," in *Boundary Influences in High-Frequency, Shallow Water Acoustics*, N.G. Pace and P. Blondel, Eds., Bath, U.K.: Univ. of Bath Press, September 2005, pp. 359–364.

[12] R. J. Soukup, G. Canepa, H.J. Simpson, J. E. Summers, and R. F. Gragg, "Small-slope simulation of acoustic backscatter from a physical model of an elastic ocean bottom," *J. Acoust. Soc. Am.*, vol. 122, no. 5, pp. 2251–2559, November 2007.

[13] J.E. Summers, R.J. Soukup, and R.F. Gragg, "Mathematical modeling and computer-aided manufacturing of rough surfaces for experimental study of seafloor scattering," *IEEE J. Ocean. Eng.*, vol. 32, no. 4, pp. 897–914, October 2007.

[14] D.C. Calvo, G. Canepa, R.J. Soukup, E.L. Kunz, J.-P. Sessarego, and K. Rudd, "Benchmarking of computational scattering models using underwater acoustic data from a corrugated wax slab," *J. Acoust. Soc. Am.*, vol. 123, pp. 3602, July 2008.

[15] V. Jaud, J.-P. Sessarego, C. Gervaise, and Y. Stephan, "Bistatic scattering from an anisotropic rough surface in water tank," in *4th International Conference on Underwater Acoustics Measurements*, Kos, Greece, June 2011, pp. 809–816.

[16] V. Jaud, J.-P. Sessarego, C. Gervaise, and Y. Stephan, "High frequency roughness scattering from various rough surfaces: theory and laboratory experiments," *Open Journal of Acoustics*, vol. 2, no. 1, pp. 50–59, March 2012.

[17] G. Real, J.-P. Sessarego, X. Cristol, and D. Fattaccioli, "De-coherence effects in underwater acoustics: scaled experiments," in *2nd International Conference on Underwater Acoustics*, Rhodes, Greece, June 2014.

[18] Ø. Midtgaard, R. Hansen, R. Sæbø, V. Myers, J. Dubberley, and I. Quidu, "Change detection using syntheric aperture sonar: Preliminary results from the Larvik trial," in *Proc. MTS/IEEE* OCEANS Conf., Kona, HI, September 2011.

[19] A.P. Lyons, “Scattering from rock and rock outcrops,” The Pennsylvania State University Applied Research Laboratory, Annual Report, September 2013.

[20] D.R. Olson and A.T. Lyons "Numerical simulation of high-frequency acoustic scattering from very rough glacially-plucked surfaces using the boundary element method," in *1st International Conference on Underwater Acoustics*, Corfu, Greece, June 2013.

[21] D.R. Olson, “High-frequency acoustic scattering from rough elastic surfaces”, PhD Thesis, The Pennsylvania State University, State College, PA, December 2014.

[22] D.R. Jackson and M.D. Richardson, *High-Frequency Seafloor Acoustics*, New York, NY: Springer, 2007.

[23] http://www.stratasys.com/3d-printers/technologies/polyjet-technology (Last viewed August 10, 2015).

[24] H. Wang, T. Ritter, W. Cao, and K.K. Shung, "High frequency properties of passive materials for ultrasonic transducers", *IEEE Trans. Ultrason., Ferroelect., Freq. Contr.*, vol. 48, no. 1, 78–84, January 2001.

[25] J. Wu, “Determination of velocity and attenuation of shear waves using ultrasonic spectroscopy", *J. Acoust. Soc. Am.*, vol. 99, no. 5, 2871–2875, May 1996.

[26] R.C. Gauss, J.M. Fialkowski, D.C. Calvo, R. Menis, D.R. Olson, and A.P. Lyons, “Moment-based method to statistically categorize rock outcrops based on their topographic features”, in *Proc. MTS/IEEE OCEANS’15 Conf. Washington*, National Harbor, MD, 2015.